Membrane Lipids Destabilize

Short Interfering Ribonucleic Acid (*siRNA)/Polyethylenimine Nanoparticles*

Yousef Nademi,[a] Tian Tang,[b] and Hasan Uludağ[a, c ,d]

[a] Department of Chemical and Materials Engineering,

[b] Department of Mechanical Engineering,

[c] Department of Biomedical Engineering, and

[d] Faculty of Pharmacy and Pharmaceutical Sciences, University of Alberta, Edmonton, Canada

Abstract

Cell entry of polymeric nanoparticles (NPs) bearing polynucleotides is an important stage for successful gene delivery. In this work, we addressed the influence of cell membrane lipids on the integrity and configurational changes of NPs composed of short interfering ribonucleic acid (siRNA) and polyethylenimine. We focused on NPs derived from two different PEIs, unmodified low molecular weight PEI and a linoleic acid (LA)-substituted PEI, and their interactions with two membrane lipids (zwitterionic 2-oleoyl-1-palmitoyl-sn-glycero-3-phosphocholine (POPC) and anionic 1-palmitoyl-2-oleoyl-sn-glycero-3-phospho-L-serine (POPS)). Our experiments showed that POPS liposomes interacted strongly with both types of NPs, which caused partial dissociation of the NPs. POPC liposomes, however, did not induce any dissociation. Consistent with the experiments, steered molecular dynamics simulations showed a stronger interaction between the NPs and POPS membrane as compared to the POPC membrane. Lipid substitution on the PEIs enhanced the stability of the NPs during membrane crossing; lipid association between PEIs of the LA-bearing NPs as well as parallel orientation of the siRNAs provided protection against their dissociation (unlike NPs from native PEI). Our observations provide valuable insight into the integrity and structural changes of PEI/siRNA NPs during membrane crossing which will help in the design of more effective carriers for nucleic acid delivery.

1. Introduction

Gene therapy involves delivery of nucleic acids (NAs) deoxyribonucleic acid (DNA) and ribonucleic acid (RNA) into cells with the purpose of modifying protein expression profile in order to alter disease progression[1]. However, effective delivery of NAs to cells is a challenging task. Various viral and non-viral vectors have been devised to enable NA delivery. Among the non-viral carriers, cationic polymers are commonly used due to their ability to form 'nano'-sized polyelectrolyte complexes with the NAs that are ideal for cell uptake. The cationic polymers protect NAs from enzymatic degradation, and facilitate their cellular uptake and endosomal escape[2]. The cationic polymer polyethylenimine (PEI) is a versatile cationic carrier that has been used since 1995 for NA delivery *in vivo* and *in vitro*[3]. PEIs form a nanoparticle (NP) with NAs *via* electrostatic interaction between the positively charged amine groups of PEIs and the negatively charged phosphate groups in the NA backbone[4]. The PEI/NA NPs enter the cells through a process that involves interaction with cell membrane molecules[5]. Cell membranes consist of a wide variety of components, but their major constituent is the lipid bilayer that acts as a physical barrier against foreign components and maintains the integrity of intracellular milieu[6].

Some PEIs in PEI/NA NP systems can exist in free form (not bound to NAs), which might destabilize membrane structures, thus contributing to the uptake of PEI/NA NPs[7]. Because of this, many experimental and simulation studies focused on the interaction of free PEIs with phospholipid bilayer of cell membrane. Among those, some studies have focused on investigating the stability of liposomes in the presence of free PEI molecules. Zhang et al[8], using sum frequency generation (SFG) vibrational spectroscopy and attenuated total-internal reflection Fourier Transform Infrared Spetcroscopy (ATR-FTIR), found that both linear PEI (lPEI) and branched PEI (bPEI) induced lipid translocation, also known as lipid "flip-flop", in anionic dipalmitoylphosphatidylglycerol (DPPG) and zwitterionic distearoylphosphatidylcholine (DSPC) lipid bilayers, while lipid translocation was higher with bPEI. Yasuhara et al.[9] proposed that PEI–lipid interactions depended on the molecular weight (MW) and stoichiometry of the PEI. Both high MW PEI (1.8 and 10 kg mol^{-1}), and low MW PEI (0.6 kg mol^{-1}) were able to induce membrane fusion [10], however, latter induce membrane fusion at wider range of free PEI

concentration. Other experimental studies proposed that PEI-lipid interactions could cause deformation and permeabilization of the lipid membrane, thus leading to enhanced exchange of material across the cell membrane [11,12].

Details of membrane deformations caused by free PEI molecules were investigated by Kwolek et al.[13] and Choudhury et al.[14] using molecular dynamics (MD) simulations. Kwolek et al[13] found that PEIs adsorbed only partially on the surface of the zwitterionic 2-oleoyl-1-palmitoyl-sn-glycero-3-phosphocholine (POPC) membrane, while they readily adhered to the anionic membrane of POPC/1,2-dioleoyl-sn-glycero-3-phosphoric acid (DOPA). Due to the electrostatic interactions and hydrogen bonding between PEIs and anionic lipid molecules, significant reorganization of the bilayer occurred in the vicinity of the polymers, which could facilitate their translocation. Choudhury et al.[14] observed that the PEI-lipid bilayer interactions were pH dependent. At low pH, PEIs were in an elongated configuration, caused by electrostatic repulsion between the protonated sites. This geometry induced formation of water/ion channels through the zwitterionic membrane of 1,2-dioleoyl-snglycero-3-phosphocholine (DOPC). No such channel was formed in the presence of unprotonated PEIs (at high pH), which possessed coil shape and remained at the bilayer-water interface.

To probe the stability of PEI/NA NPs in contact with cell membranes, experimental studies have focused mainly on the role of cell-surface glycosaminoglycans (GAGs). GAGs carry high anionic charge density, and are present on the surface of most cells[15]. Sulfated GAG species such as chondroitin sulfate (CS), heparin sulfate (HS), dermatan sulfate (DS) and keratin sulfate (KS) carry higher negative charges that vary in density and position[16]. Hyaluronic acid (HA), on the other hand, is not sulfated and bears the least net negative charge among GAGs[16]. It has been suggested that GAGs compete with the NAs in binding to PEIs, and disrupt the integrity of PEI/NA NPs intended for cell uptake [17,18]. Meneksedag-Erol et al. [5] based on MD simulations proposed a 5-stage mechanism for heparin mediated dissociation of PEI/siRNA (short interfering RNA) NPs: (*i*) binding of heparin to the NP, (*ii*) separation of surface PEIs, (*iii*) detachment of bridging PEIs, (*iv*) misalignment between constituent siRNAs, and (*v*) disintegration of the NP. Ernst et al [19] studied the efficiency of transfection of various polymer/DNA NPs including the PEI/DNA

NPs in presence of various liposomal surfactants (DPPG, 1-palmitoyl-2-oleoyl-sn-glycero-3-phosphoglycerol (POPG), 1,2-dipalmitoyl-sn-glycero-3-phosphocholine (DPPC), POPC, and 1-palmitoyl-2-oleoyl-sn-glycero-3-phosphoethanolamine (POPE)) using different cell lines including cultured human airway epithelial cells (16HBE14O-), COS7 cells and porcine primary airway epithelial cells. Lipids with PC head groups showed some inhibitory effect on the transfection of PEI/DNA NPs, while those with PE head groups had little or no effect. Lipids with negatively charged PG head groups, on the other hand, strongly inhibited the transfection, which was attributed to possible conformational changes of the NPs leading to different NP sizes unsuitable for transfection.

While some studies probed the integrity of lipid membrane exposed to free PEIs, whether the lipid membrane components might affect the integrity of PEI/NA NPs and alter their configuration has been not explored. Others simulated PEI/NA NP interactions with lipidic membranes, but not NP stability as it is passing through the membrane[20]. Coarse-grained simulations were reported on the interaction of NP with membrane, in addition to a review paper that addressed strategies to tailor the spatial distribution and ordering of the NP at the interfaces of various systems [21–23]. To the best of our knowledge, this is the first atomistic-level study that focuses on the stability of PEI/siRNA NPs in contact with representative lipidic membranes. Experiments and steered molecular dynamics (SMD) simulations were combined to examine the role of lipid molecules on the integrity of NPs formed by siRNA and PEI. Zwitterionic POPC and anionic 1-palmitoyl-2-oleoyl-sn-glycero-3-phospho-L-serine (POPS) membranes were used as model cell membranes. A native (unmodified) PEI and a PEI substituted with linoleic acid (LA) were adopted to investigate the effect of lipid modification, since such lipid modification on PEI has shown beneficial effects in siRNA delivery [24,25].

2. Materials and Methods

2.1 Materials

POPC and POPS lipids were purchased from Avanti Polar Lipids. Heparin sodium from porcine intestinal was purchased from Sigma-Aldrich (St. Louis, MO). The negative control siRNA was purchased from Ambion (Austin, TX). SYBR Green II RNA gel stain (10 000X concentrate in DMSO) was purchased from Cambrex Bio Science (Rockland, ME). Two kDa PEI and PEI-LA polymers were developed in our group, and the synthesis procedure was previously described [26].

2.2 Experimental Procedures

Binding Assay. The binding ability of native PEI and LA-modified PEI with siRNA was investigated using SYBR Green II dye binding assay in triplicates. Briefly, 0.42 µg of siRNA (in ddH2O) was incubated with various concentrations of the indicated polymers (in ddH_2O) for 30 min. Then, 100 µl of SYBR Green II solution (1:10000 dilution in TAE buffer) was added to the mixture. The fluorescence intensity was measured using a Fluoroskan Ascent Microplate Fluorometer with λ_{ex}= 485 nm and λ_{em} = 527 nm. The percentage of bound siRNA was estimated on the basis of the fluorescence intensity relative to the siRNA sample in the absence of polymer (fluoresecence values taken as 0% binding).

Preparation of Liposomes. POPS and POPC liposomes were prepared using extrusion technique. First, lipids were weighted to the desired amounts and dissolved in chloroform to obtain 4 mg/mL solutions. Then, the solvent was evaporated under reduced pressure by a rotary evaporator. The lipid film so formed was re-suspended in nuclease free water and vortexed with a final lipid concentration of ~1 mg/mL. The resulting liposomes were extruded ten times through membrane syringe filters with 220 nm pores.

Light Scattering and Zeta Potential Measurements. Mean hydrodynamic diameter, polydispersity (PDI), and ζ-potential of liposomes were measured using dynamic light and electrophoretic light scattering methods with a Zetasizer (Nano ZS; Malverin instruments, UK), and the measurements were performed in triplicates.

Electrophoretic Mobility Shift Assay (EMSA). EMSA was performed to assess the stability of PEI/siRNA NPs in the presence of POPS and POPC liposomes. The samples were prepared by mixing 0.28 μg of siRNA (in ddH_2O, pH = 7) with unmodified and LA-modified PEI at PEI:siRNA weight ratios of 0.3 and 1, respectively, for 30 min at room temperature. The selected weight ratios corresponded to 100% binding between siRNA and polymers (based on SYBR Green II binding assay above). Then, various concentrations of liposomes were added to the samples and incubated for one additional hour, after which 5 μL of 40% glycerol was added to the samples, and the samples were run on a 0.4% agarose gel containing SYBR Green II using 100 V for 30 min. The resulting gels were visualized under UV-illumination. As a control for complete dissociation, heparin was added to samples where no liposome was present, and it was analyzed by EMSA as above. A band in which siRNA without any polymers added was also used as a reference. The dissociation percentage was estimated on the basis of the fluorescence intensity of the identified bands relative to the free siRNA band. Gels were run in at least 2 independent assays.

2.3 Simulated Systems and Procedure

Two types of NPs were simulated, each consisting of 2 siRNA molecules and 6 bPEIs. The siRNA in the simulations had sense strand of 5'-CAGAAAGCUUAGUACCAAATT-3' with an antisense strand of 5'-UUUGGUACUAAGCUUUCUGTC-3'. This siRNA sequence was specific for P-glycoprotein silencing [27] and it was used in our previous simulation studies. It consists of 42 nucleotides with a total charge of −40 in its fully deprotonated state. The simulated native bPEI has a molecular weight of 1874 Da and is composed of 43 amine group. Twenty of them are protonated, corresponding to the protonation ratio of 47%, which is within the reported range (10 to 50% [28–32]) of protonation ratio for PEI at physiological pH . Hereafter the NP formed by the 2 siRNA and 6 native PEIs is referred to as PEI NP. The other simulated NP is referred to as PEI-LA NP, where each PEI is modified with 3 LA substitutions. The substitution level is in the practical range used for siRNA delivery[24]. The chemical structures of simulated polymers as well as model membrane lipids are shown in Fig. 1.

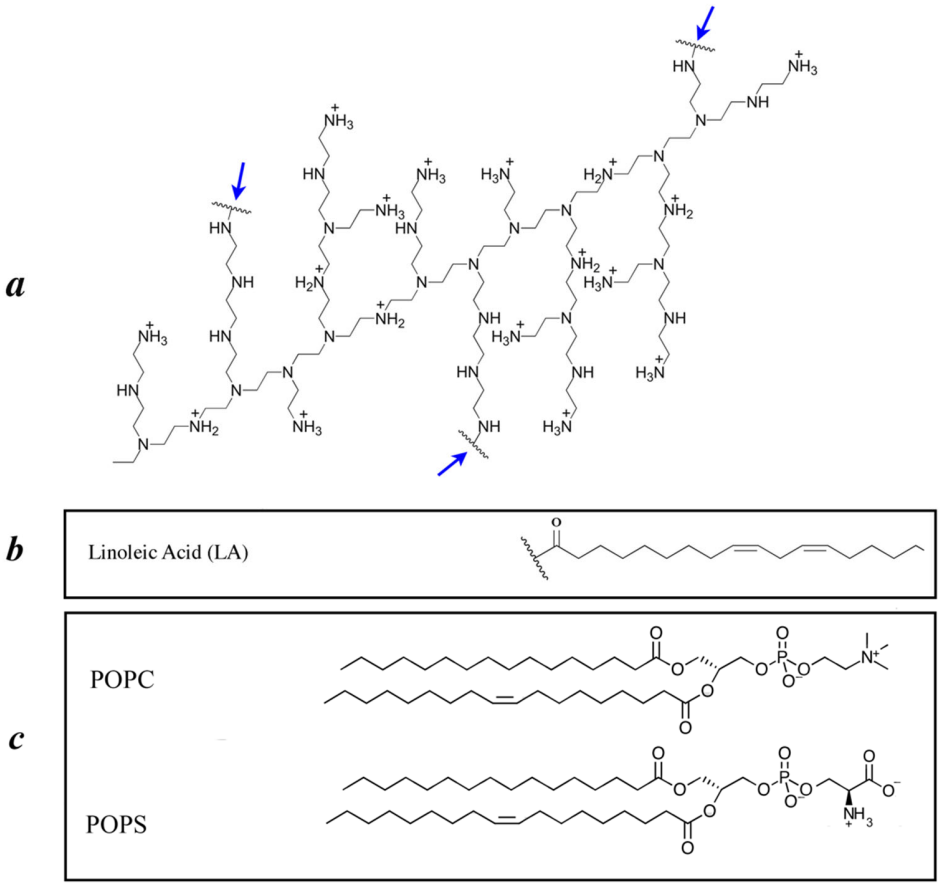

Figure 1. Molecular structure of (a) native PEI, where lipid substitution sites are shown with blue arrows, (b) LA to be substituted to native PEI, and (c) POPC and POPS molecules.

The initial structures of NPs as well as POPC membrane were adopted from our previous study [33]. Specifically, each NP was subjected to 50 ns of MD simulation, and the equilibrated structure was adopted as the initial configuration for subsequent SMD simulations in this work. The anionic bilayer of 1016 POPS molecules were constructed using Membrane Builder [34] in CHARMM-GUI [35,36]. To equilibrate the membrane structure, the POPS lipids were solvated with TIP3P [37] water molecules and 150 mM KCl, and then subjected to 50 ns MD simulation until the area per lipid reached 57.26 ± 0.43 $Å^2$ (data collected from last 20 ns), which is in agreement with the values reported in literature [38]. The final configuration of the POPS lipid bilayer was used as the input structure for SMD simulation of the NPs. SMD systems were

prepared by placing each NP above the membrane so that the center of mass (COM) distance between the membrane and the NP was 8 nm. Initial orientation of each NP was selected in a way that the axes of its siRNAs were almost perpendicular to the membrane surface. Following solvation with TIP3P [37] water and 150 mM KCl, each of the four membrane-NP systems was equilibrated for 6 ns with a harmonic restraint of 10 $kcal\ mol^{-1}\ Å^{-2}$ exerted on the non-H atoms of the NP. The equilibrated membrane-NP systems were then used for SMD simulations. Specifically, COM of the NP was attached to a dummy atom *via* a virtual spring, which was pulled with a constant velocity along *z* direction (perpendicular to the membrane surface), and the force between the COM of the NP and the dummy atom was calculated. Results reported in this work are on the basis of pulling speed $v = 5\ Å\ ns^{-1}$ and spring constant $k = 5\ kcal\ mol^{-1}\ Å^{-2}$ according to the "stiff-spring approximation" [39]. Although pulling speeds as low as $0.1\ Å\ ns^{-1}$ have been used in the literature to determine the potential of mean force [39–41], much larger pulling speeds (as high as $100\ Å\ ns^{-1}$) have also been used for qualitative assessment and for making comparisons among different system[42–45]. In a previous work [33], we investigated the effect of pulling speed and demonstrated the suitability of using $v = 5\ Å\ ns^{-1}$ for studying structural changes of NPs during membrane penetration. The length of each SMD simulation is 34 ns for the NP to travel a total distance of 170 Å . Detailed information on the simulated systems is provided in Table 1.

Table 1. Details of simulated systems in this study.

System	Number of atoms	Size of simulation box (Å^3)	Lipid no./type on each PEI	PEI/siRNA charge ratio	Simulation time (ns)
PEI NP-POPS	988688	170 × 171 × 340	None	1.5	34
PEI-LA NP- POPS	988662	170 × 171 × 340	3 LA	1.27	34
PEI NP-POPC	782077	170× 172 × 270	None	1.5	34
PEI-LA NP- POPC	778742	170× 172 × 270	3 LA	1.27	34

2.4 Simulation Details

Force field parameters for the PEIs were previously generated and validated by our group [25] based on the CHARMM General Force Field. For other molecules, CHARMM 36 [46,47] force field was used. Molecular simulation package NAMD [48] was used to perform the simulations in NPT ensemble. Time steps of 2 fs, periodic boundary conditions, and Particle Mesh Ewald [49] (PME) to calculate long-ranged electrostatic interactions were used for all simulations. The cut off distance was 12 Å for van der Waals and short-ranged electrostatic interactions, and SHAKE [50] algorithm was employed to constrain bonds involving H atoms. The temperature (310 K) was controlled using Langevin dynamic thermostat. To maintain the pressure (1 bar), Nose-Hoover Langevin barostat with a damping time scale of 100 fs and a Langevin piston oscillation period of 200 fs were used [51,52]. Visualization and analysis of simulations trajectories were performed using VMD [53].

3. Results

3.1 Experimental Determination of PEI Binding to siRNA

The percentage of bound siRNA as a function of PEI:siRNA weight ratio is shown in Fig. 2. For both polymers, with increase in PEI:siRNA ratio, the fraction of bound siRNA was increased. However, 100% binding was achieved at different PEI:siRNA weight ratios, 0.3 for native PEI and 1.0 for PEI-LA. The results showed that LA substitution impeded siRNA binding to the cationic PEI. Similar observation was previously reported by Aliabadi et al [24]. It is worth noting that as lipid substitutions were introduced, the fraction of 'protonable' Ns was reduced so that PEI-LA was less charged as compared with its native counterpart. For the PEI structure shown in Fig. 1a where 3 LA substitutions were introduced to each PEI, to obtain the same cationic: anionic charge ratio, the PEI:siRNA weight ratio would have to be 1.45 times higher for PEI-LA. Since binding between siRNA and PEI strongly relies on their electrostatic interactions, it is not surprising to see a larger weight ratio required for PEI-LA to achieve 100% binding. For this reason, the dissociation assays were carried out using PEI:siRNA weight ratios that corresponded to 100% binding (0.3 and 1 respectively for PEI and PEI-LA), instead of using the same weight ratio.

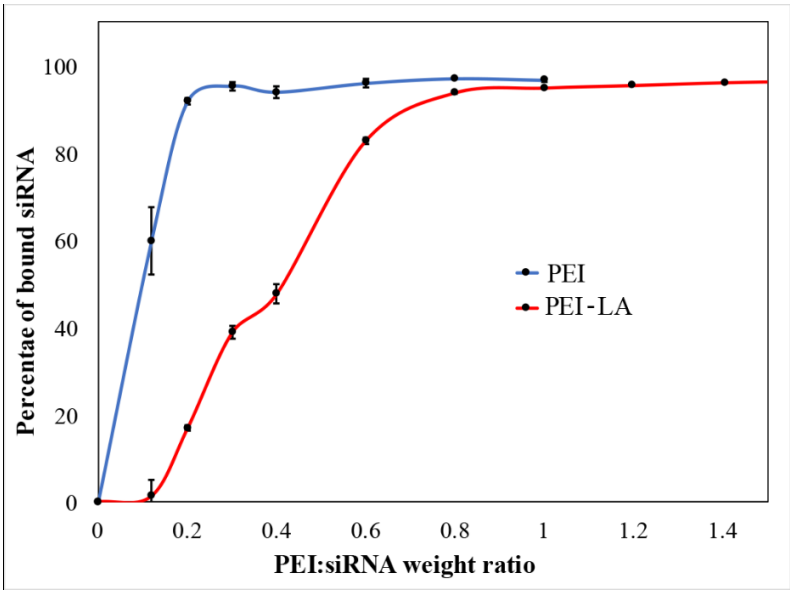

Figure 2. Percentage of bound siRNA as a function of the PEI:siRNA weight ratio from SYBR Green II binding assay for PEI (**blue**) and PEI-LA (**red**).

3.2 Liposome Characterization and Dissociation Assay

The hydrodynamic diameter, polydispersity index and ζ-potential of the liposomes are shown in Table 2. The size of POPC liposomes was smaller than the POPS liposomes. As expected, the ζ-potential of the POPS liposomes was noticeably lower than the POPC liposomes due to the presence of the additional carboxyl group in POPS. Because of lower ζ-potential and presence of -COOH in the POPS liposomes, stronger interaction is expected between cationic PEI/siRNA NPs and POPS liposomes than between PEI/siRNA NPs and POPC liposomes. The size and ζ-potential of PEI/siRNA NPs were not determined in this study, since our group previously reported them to be ~200 nm and ~ 8 mV, respectively [24,54].

Table 2. Hydrodynamic diameter (d_z), polydispersity index (PDI) and ζ-potential (ξ) of POPS and POPC liposomes.

Liposome	d_z (nm)	PDI	ξ(mV)
anionic POPS	202.3 ± 4.0	0.262 ± 0.01	−32.53 ± 2.22
zwitterionic POPC	163.6 ± 8.0	0.240 ± 0.03	−18.73 ± 1.71

To investigate the effect of membrane lipids on the integrity of PEI/siRNA NPs, EMSA was performed by adding liposomes to fully bound PEI/siRNA NPs. The amount of liposome was gradually increased, and the dissociation percentage was measured (Fig. 3). With the addition of POPS liposomes, the NPs showed some level of dissociation: e.g., with 4 µg of POPS liposomes, ~87% and ~47% dissociation was obtained with PEI and PEI-LA NPs, respectively. However, complete dissociation was not observed with further addition of POPS liposomes. The dissociation of PEI-LA NPs with POPS liposomes was consistently lower than the PEI NPs. The addition of POPC liposomes did not lead to significant dissociation as the percentage of unbound siRNA remained low (~10 and ~6% for PEI and PEI-LA NPs, respectively), indicating clear differences between the abilities of POPS and POPC liposomes to cause NP dissociation. To find an atomistic insight on configurational changes caused by liposomes – NP interactions, SMD simulations were utilized and the results are presented in the following section.

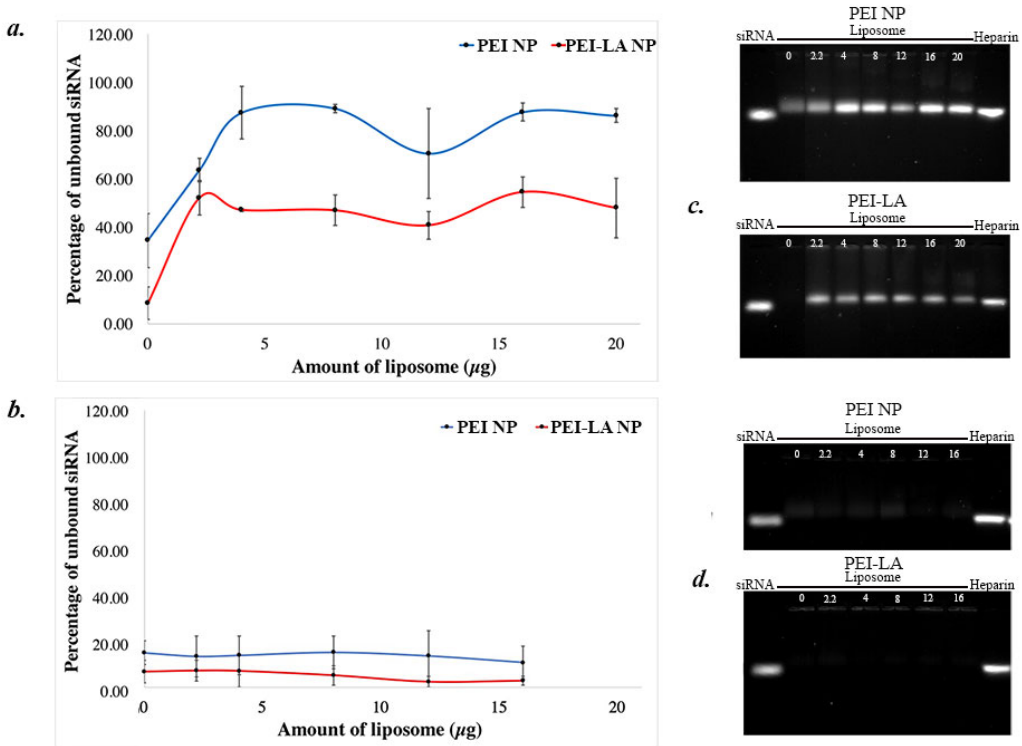

Figure 3. Percentage of unbound siRNA as a function of amount of (a) POPS (b) POPC liposomes. EMSA images of siRNA release from NPs in presence of (c) POPS and (d) POPC liposomes.

3.3 Steered Molecular Dynamics Simulations

Fig. 4 shows the force profiles during SMD simulations, as a function of COM position of the NP. The original locations of undeformed membrane surfaces are marked with the dashed lines. Depending on the distance of the NP from the membrane, the crossing process was divided into 4 stages: approach (-80 to -60 Å), attachment (-60 to 0 Å), embedment (0 to 50 Å), and detachment (50 to 90 Å). Side-view snapshots of the NPs and the membrane representative of each of these four stages are shown in Fig. 5. During the approach stage, the applied force was relatively constant and low, corresponding to the dissipative force from the solvent that resists the movement of the NP. In the attachment stage, the membrane applied an additional force against the NP movement, which continued to increase during the embedment stage until it reached a maximum value. Afterward a pore is formed in the membrane structure, and the force decreased during detachment. For both types of NPs, the magnitude of the force was higher for the POPS membrane during attachment stage and afterwards, suggesting its stronger interaction with the NPs. For the same membrane, the force profiles for the PEI NP and PEI-LA NP were overlapping during the approach, attachment and most of the embedment (up to ~40 Å) stages. However, during the detachment stage, the force was higher for PEI-LA NP, indicating stronger interaction between the PEI-LA NP and the membrane.

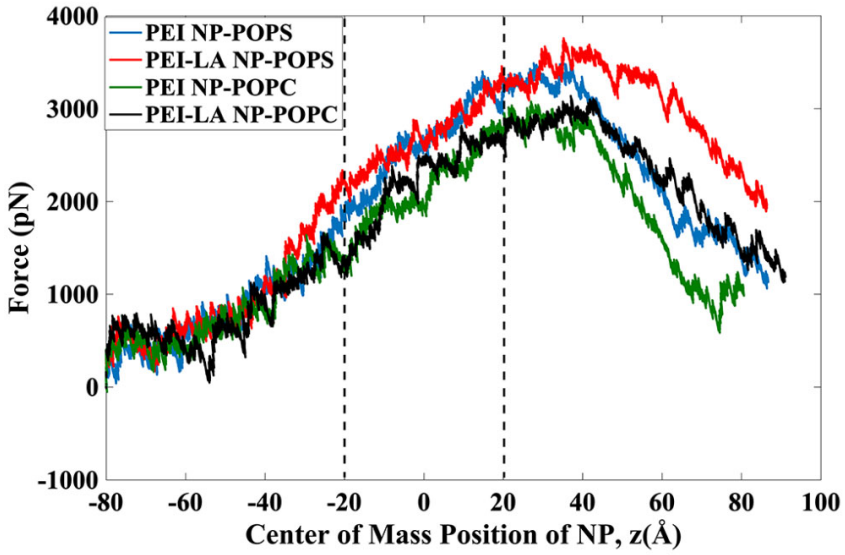

Figure 4. Force vs. COM position of the NP during SMD. The two dashed lines denotes the surfaces of the initial undeformed membrane.

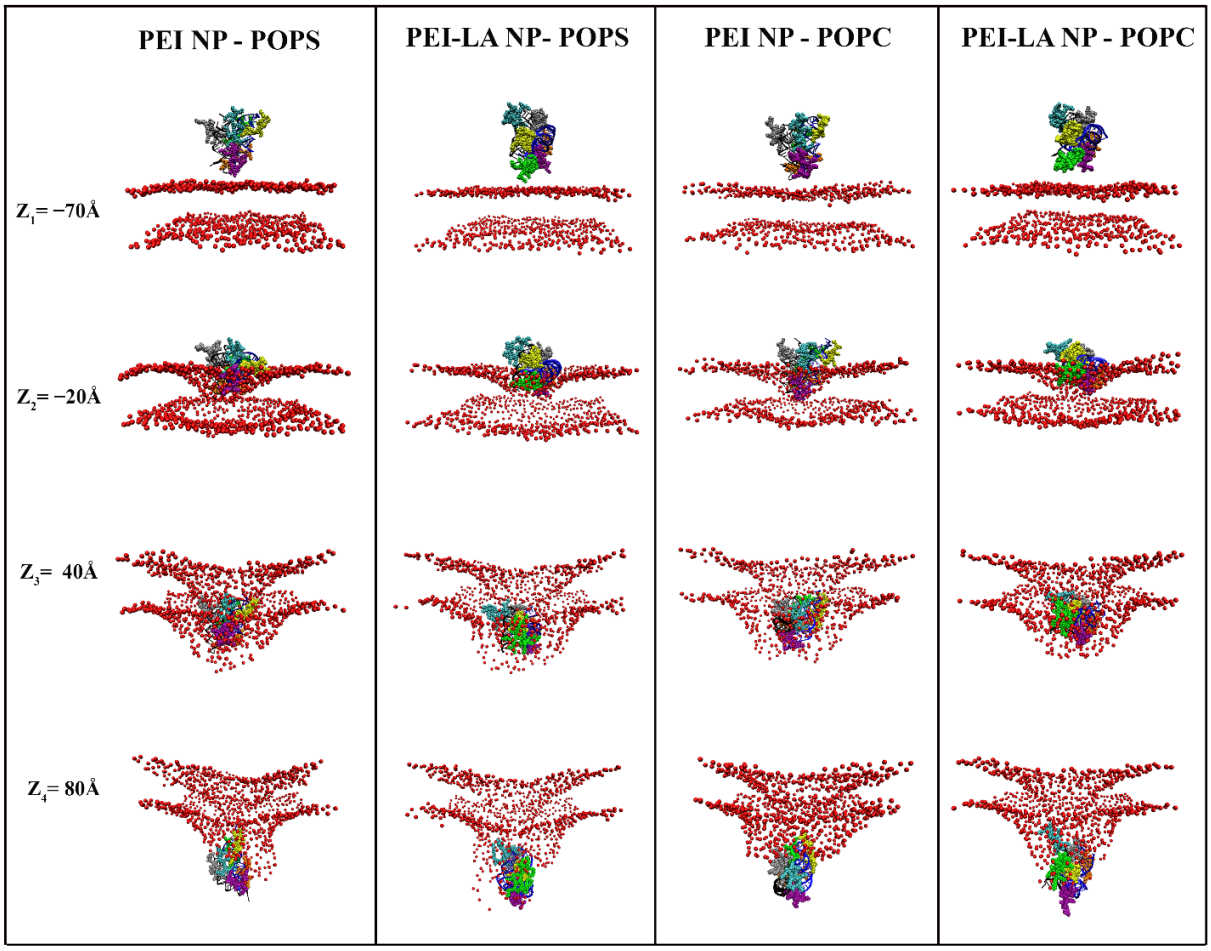

Figure 5. Side-view snapshots of the NP and membrane at different instants of the SMD simulations. Different PEIs and siRNAs are represented by different colors. For clarity, water and ions are removed and only the phosphate (P) atoms of the membrane are shown (in red). The four snapshots, from top to bottom, correspond to the four stages of NP penetration, namely approach, attachment, embedment, and detachment.

The integrity of PEI/NA NPs highly depends on the binding between siRNAs and PEI molecules. Fig. 6 and Fig. 7 show the number of PEI N atoms within 4 Å of any N/O atoms of siRNA as a function of COM position of NP for POPS and POPC membranes, respectively. The use of 4 Å as a criterion is based on the distance in which a direct hydrogen bond between PEI amines and siRNA N/O could be formed [55,56]. The number of hydrogen bonds (HBs) between PEIs and siRNA molecules were shown in Fig. S1 and Fig.

S2, which show the same trends. The results in Fig. 6 and Fig. 7 (one subplot for each PEI) thus represent the number of contacts the PEIs make with the siRNAs. Each subplot has two curves corresponding to the two siRNA molecules. A PEI is defined as' bridging' if it has at least one N atom within 4 Å of any N/O atoms of both siRNA molecules, i.e., it is simultaneously attached to both siRNAs. Other PEI molecules are considered peripheral, as they are attached to only one of the siRNAs without forming polyion bridges between the two. In all systems, four PEIs were bridging (labeled as PEI-1, PEI-2, PEI-3 and PEI-4) and two PEIs were peripheral (labeled as PEI-5 and PEI-6). For the POPS membrane and PEI NP (Fig. 6a), interactions of bridging PEIs with siRNAs showed little changes during approach, attachment and embedment. However, during detachment, bridging performance of 3 PEIs (PEI-1, PEI-2, and PEI-3) were weakened, demonstrated by their reduced number of contact with one or both of the siRNAs. By the end of the detachment process, PEI-2 and PEI-3 had almost completely lost their interactions with siRNA-2, starting to change from bridging to peripheral. Peripheral PEIs (PEI-5 and PEI-6) behaved similarly, where their interactions with siRNAs were increased during attachment and embedment and decreased during detachment. However, the decrease was more profound for PEI-6. For the POPS membrane and PEI-LA NP (Fig. 6b), interactions of 2 bridging PEIs (PEI-1 and PEI-2) with siNRAs barely changed during all stages, while the other 2 bridging PEIs (PEI-3 and PEI-4) displayed a dynamic trend. For PEI-3, number of contacts it had with both siRNAs increased during penetration. PEI-4 also showed increased interaction with siRNA-2; its interaction with siRNA-1 first decreased during attachment and embedment, but recovered during detachment. Interactions of the peripheral PEIs (PEI-5 and PEI-6) with siRNAs were stable and showed little changes.

For the POPC membrane and PEI NP (Fig. 7a), bridging PEIs showed a fluctuating trend, however, no sign of weakened interaction was observed compared with the initial number of contacts. Peripheral PEI-5 showed an overall increasing interaction with siRNA-1, while the interaction of peripheral PEI-6 with siRNA-2 had a decreasing trend during detachment. For the POPC membrane and PEI-LA NP (Fig. 7b), bridging PEIs maintained their interaction with siRNAs (PEI-4 temporarily lost contact with siRNA-1 during embedment but the interaction was recovered during detachment). Peripheral PEI-5 had a

stable interaction with siRNA-1 while there was slight decrease in the interaction between PEI-6 and siRNA 2.

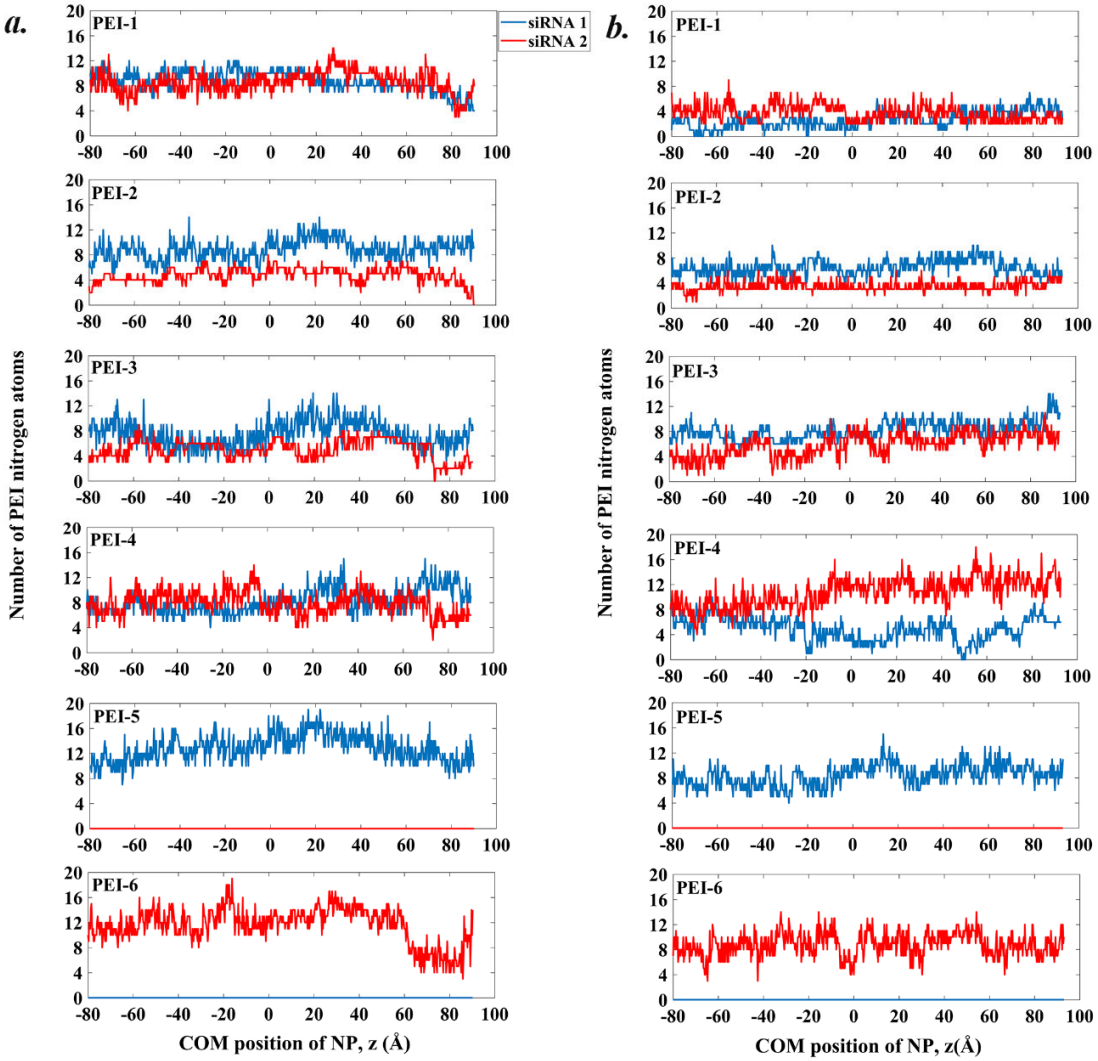

Figure 6. Number of PEI Ns within 4 Å of any siRNAs N/O atoms as a function of COM position of NP while crossing the POPS membrane, (a) PEI NP and (b) PEI-LA NP.

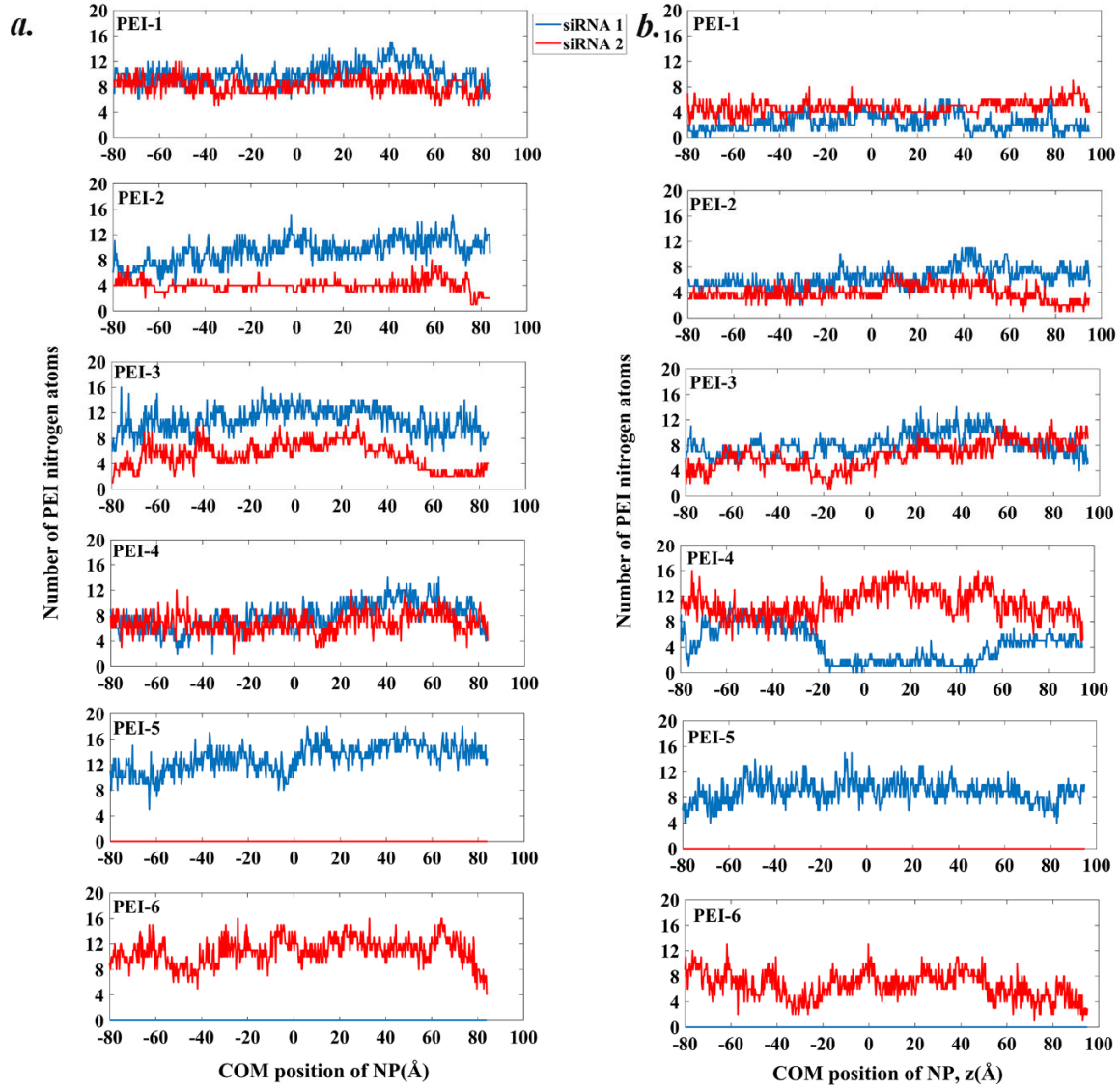

Figure 7. Number of PEI Ns within 4 Å of any siRNAs N/O atoms as a function of COM position of NP while crossing the POPC membrane, (a) PEI NP and (b) PEI-LA NP.

These changes in PEI configurations could lead to structural changes in NP, thereby affecting the integrity of NP during penetration. Hence, configurational changes in NPs were quantified by calculating the gyration radius (R_g) of the NPs, and the COM distance and relative angle between the two siRNAs. Results are shown in Fig. 8 for the POPS (left panel) and POPC (right panel) membranes. With POPS membrane, R_g (Fig. 8a) was relatively constant for both NPs during the approach stage, decreased during

attachment and embedment, and increased during detachment. This suggests that each NP experiences some level of compaction during attachment and embedment, while "recovering" from their compacted structure during detachment.

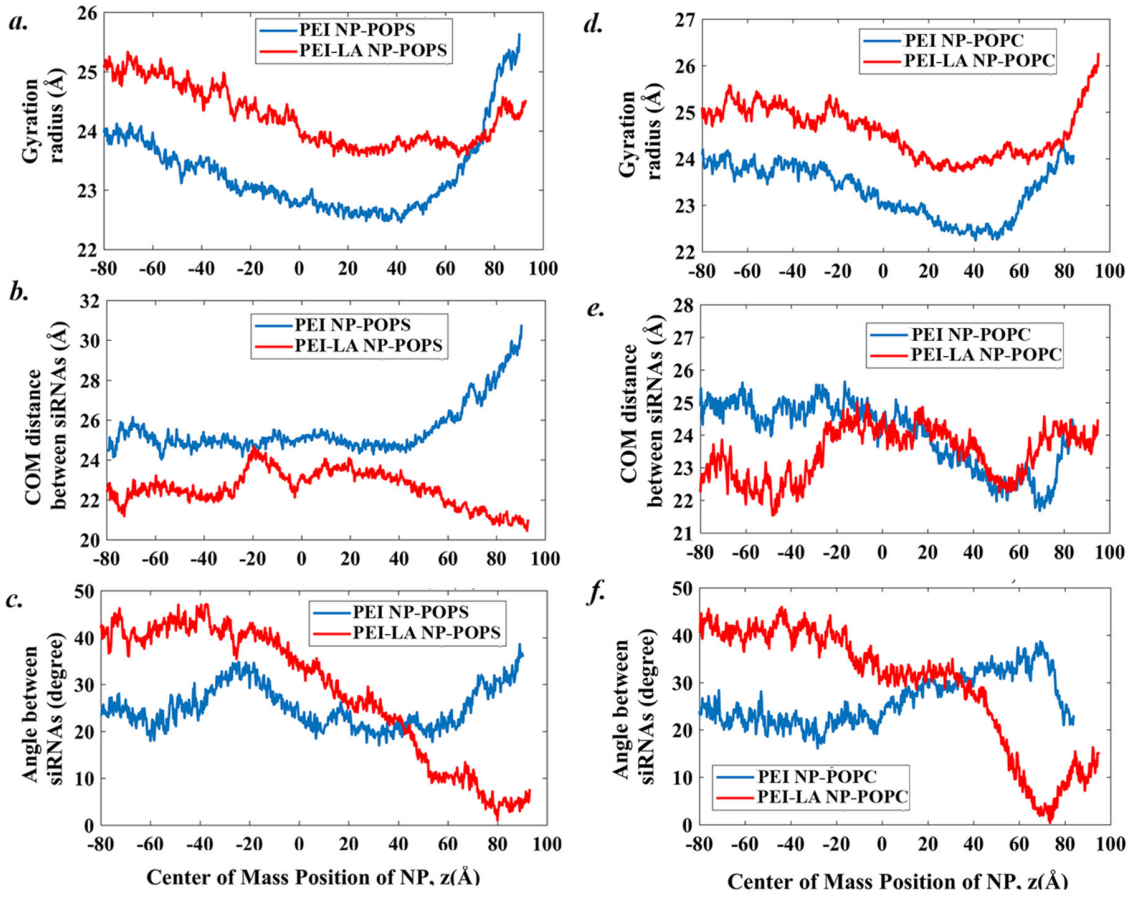

Figure 8. Structural parameters for NPs crossing the POPS (left panel) and POPC (right panel) membranes: (a, d) Gyration radius of the NP, (b, e) COM distance between the two siRNAs, and (c, f) the relative angle between the two siRNAs, each as a function of the COM position of the NP.

The compaction of NP could occur in two ways, first through the reduction in COM distance between the two siRNAs, and second through the contraction of the PEIs. The COM distance between the 2 siRNAs is plotted in Fig. 8b. For both types of NPs, the COM distance hardly changed during the approach, attachment and embedment. During detachment, distinct behaviors were observed for the two NPs: while the COM distance increased significantly for PEI NP, it decreased for PEI-LA NP. To quantify the role of

PEIs on the observed NP compaction and recovery, R_g of each NP are plotted for the POPS (left panel) and POPC (right panel) membranes (Fig. 9). For POPS membrane and PEI NP, R_g of all PEIs were constant during the approach stage. During attachment and embedment, R_g of 2 bridging PEIs (PEI-2 and PEI-4) and 1 peripheral PEI (PEI-6) remained constant while that of the other 2 bridging PEIs (PEI-1 and PEI-3) and 1 peripheral PEI (PEI-5) decreased. Together with the stable COM distance between the two siRNAs, it can be concluded that the compaction of the PEIs gave rise to the overall reduction in the R_g of the NP. During detachment, R_g of 3 PEIs (PEI-2, PEI-4, and PEI-5) were almost constant whereas R_g of the other 3 PEIs experienced slight increase. The increase, compared with the change in COM distance between the siRNAs, is small, and the increase in R_g of the NP was primarily due to the increased separation of the siRNA. For POPS and PEI-LA NP, similarly, R_g of all PEIs were constant during the approach stage. During attachment and embedment, R_g of 3 PEIs (PEI-2, PEI-3 and PEI-5) showed a decrease, while R_g of 1 PEI (PEI-4) displayed a slight increase. R_g of PEI-6 showed a fluctuating trend, where it first decreased up to the COM position of 0 Å, and then increased afterward. Considering the insignificant changes in COM distance between the siRNAs, the compaction of NP is again through the contraction of PEIs. During detachment, R_g of 4 PEIs (PEI-1, PEI-3, PEI-5, PEI-6) show an increase, while changes in R_g of the other PEIs was small. Considering a slight decrease in the COM distance between siRNAs, the recovery of the compacted NPs was mostly caused by the relaxation of the PEIs.

Fig. 8c shows the relative angle between the two siRNAs for POPS, as a way to quantify changes in siRNA alignment during membrane penetration. Previous studies suggested that misalignment may impact NP integrity by increasing the accessible area between the two siRNAs, which allows destabilizing compounds to interact with the NP core [5]. The relative angle (θ) was defined and calculated based on two vectors, one in each siRNA. θ = 0° indicates parallel orientation, whereas θ = 90° corresponds to perpendicular orientation of the siRNAs. For PEI NP, θ underwent some initial fluctuations but showed an increasing trend during detachment, corresponding to increased misalignment between the two siRNAs. For PEI-LA NP, θ was stable during approach but gradually decreased throughout the attachment, embedment and detachment stages. Eventually the two siRNAs formed an almost parallel orientation

(θ~4°). Such an alignment limits the interaction between membrane molecules and the PEIs at the center of the NP serving as polyion bridges, thereby protecting the PEI-LA NP from dissociation.

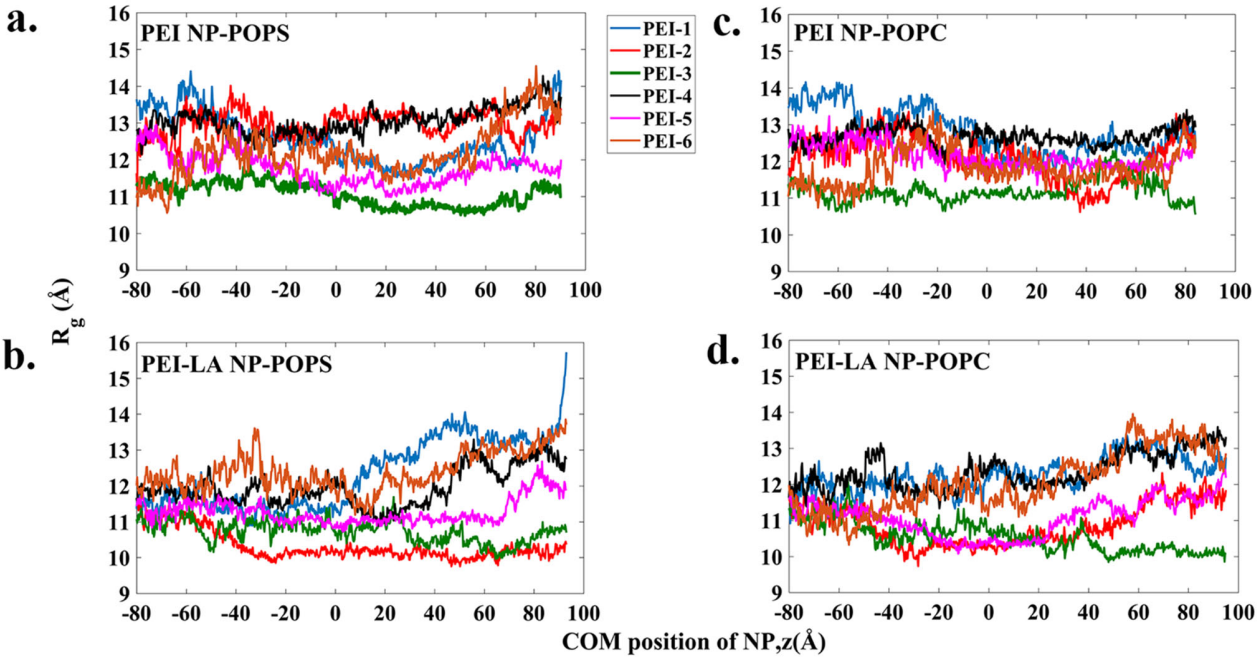

Figure 9. Gyration radius of the PEIs as a function of COM position of NP crossing the POPS (left panel) and POPC (right panel) membranes.

Corresponding results for the POPC membrane are shown in Fig. 8d, e, f and Fig. 9c, d. Table S1 summarizes the changes in the structural parameters for the two types of NPs and two membranes. The key differences between POPC and POPS membranes are shown in red color, which mainly occur during detachment. For POPC in this stage, R_g of PEI NP increased to about the initial value, while it increased to 1 Å more than the initial value for the PEI-LA NP. The COM distance between siRNAs of both NPs exhibited no significant increase, indicating NPs retained their integrity. No noticeable change in θ was observed for PEI NP, while PEI-LA NP again formed an almost parallel orientation. Comparing the results in the right panels of Fig. 8 and Fig. 9, for PEI NP there was a clear correlation between R_g of the NP and the COM distance between the siRNAs, while R_g of individual PEIs were almost constant. This suggests that the compaction and recovery of the PEI NP while crossing the POPC membrane were both due to

changes in the siRNA separation. On the other hand, the compaction and recover of PEI-LA NP depended more strongly on the configurational changes of the PEIs.

4 Discussion

The stability of PEI/siRNA NPs en-route to cells is crucial for an effective therapeutic outcome [57]. If the NP integrity is disrupted before uptake, the siRNAs will get exposed to surrounding environment prematurely, and the efficacy of delivery will reduce significantly [5]. Approximately 50% of cell surface is composed of lipids including anionic and zwitterionic species [58]. NPs during their cellular uptake are bound to interact with the charged lipidic groups[59–64]. It has been suggested that DNA is released from lipoplexes through electrostatic neutralization of cationic membranes by anionic lipids [61]. To assess NP integrity in the presence of membranes' lipids, representative anionic (POPS) and zwitterionic (POPC) liposomes have been employed in this study. The results from ζ-potential measurements confirmed that POPS liposomes had higher negative charge than the POPC liposomes, which provide stronger electrostatic interaction with cationic NPs. Experiments of Kwolek et al.[13] on interaction between bare PEIs and liposomes showed that cationic PEIs did not interact strongly with zwitterionic POPC liposomes, and that the change in the ζ-potential of POPC liposomes treated with PEIs was insignificant. On the contrary, ζ-potential of the anionic liposomes of DOPA/POPC became positive after the addition of PEIs, indicating adsorption of the PEIs on the liposome surface. Recently, Gurtovenko[20] using MD simulations investigated the interactions between DNA/PEI NP and POPC membrane. In line with experimental observations, their simulations showed that the free energy gradually increased as the NP approached the surface of POPC membrane, indicating lack of attractive NP/membrane interactions. In our work, because of stronger interaction between anionic liposome and cationic NPs, POPS liposomes caused partial dissociation of both types of NPs in the EMSA experiments, while no dissociation was observed with the zwitterionic POPC liposomes. Our SMD simulations showed that both membranes induced configurational changes in both NPs. However, in line with the experiments, the structural changes caused by POPC was small while the POPS membrane

significantly disturbed the structure of simulated NPs, evidenced by substantial increase in their siRNAs separation distance.

Besides lipids, the cell membrane contains other molecules that can interact with polymeric NPs to affect their dissociation. An example of such molecules is GAGs, among which heparin is known for its ability to destabilize polymeric NPs [54]. Liposome-induced dissociation may follow a different process than dissociation caused by the GAGs such as heparin. With increasing concentration of GAGs, complete disintegration of the NA cargo is common [18,54]. On the contrary, even at highest concentrations of liposomes used here, complete dissociation was not observed in our work.

The presence of different membrane lipids can affect the resistive forces against the NP penetration. From atomistic point of view, these resistive forces originate from several types of interactions that stabilize the lipidic membranes. Interfacial tension caused by hydrophobic effect, steric repulsion between aliphatic chains, van der Waals interactions, HBs and electrostatics in the lipids' head group region, to name a few [65]. Here, since POPS and POPC membranes are difference from each other only by a -COOH group on POPS, stronger intermolecular interactions caused by formation of more HBs between POPS lipids is expected, consistent with the difference in the phase transition temperature of 13[66] and -3 °C[67] for POPS and POPC, respectively. The extra HBs can be formed between O of -COOH and hydrogen of $-NH_2$ on the adjacent lipid. Consistently, our simulations showed that resistive force for NP penetration into the POPS membrane was higher than the POPC membrane. Additionally, the presence of -COOH on POPS facilitates formation of more HBs between its surface and NP as quantified in Fig. S2, which provided additional resistance against the NP penetration. The HB curves mostly correlate with the force profiles, with higher number of HB leading to larger force. An exception to this was the PEI NP-POPS and PEI-LA NP-POPC systems. While the number of HBs is higher for the former system, their associated force profiles were comparable during the detachment stage. During detachment, R_g of the NPs in the PEI NP-POPS and PEI-LA NP-POPC systems were ~25.5 and ~26.5 Å (Fig. 8a, d), respectively. Considering stronger membrane deformation caused by the larger size of PEI-LA NP penetrating into the POPC membrane, the

results suggest that more lipid-lipid interaction between POPC lipids needs to be broken, thereby increasing the force in the PEI-LA NP-POPC system.

Lipid substitution on PEIs can affect the stability of NPs and their ability to resist dissociation. We and others unequivocally demonstrated that binding of bare PEI to NAs in solution is superior to lipid substituted PEIs at the same PEI:siRNA ratio. However, dissociation of the NPs by POPS liposomes was easier for the PEI NP compared to the PEI-LA NP. It has been suggested that integrity of PEI/NA NPs are highly dependent on polyion bridging and its strength, where PEIs establish contact with multiple NA[68]. Fig. 10 shows, for each bridging PEI in each simulated system, changes in its average number of N atoms within 4 Å of any N/O atoms of the siRNAs, based on calculations for the first and last 5 Å of the penetration process. For both membranes, bridging PEI Ns of PEI-LA NP either maintained or increased their interactions with siRNAs, while bridging PEI Ns of PEI NP behaved differently for the two membranes. For the POPS membrane, interaction of PEI-1 Ns of PEI NP with siRNAs was weakened considerably, while the total number of N of PEI-2 and PEI-3 in close contact with siRNAs remained relatively constant. However, the bridging performance of these two PEIs were weakened, as shown in Fig. 6a, and they showed trend of becoming peripheral rather than remaining bridging. For the POPC membrane, on the other hand, bridging PEI Ns of PEI NP retained their interaction with both siRNAs. Our SMD simulations of NP penetration through the POPS membrane also showed insignificant changes in the angle between the two siRNAs in the PEI NP, accompanied by a large increase (up to 20%) in siRNA COM distance during detachment. On the other hand, PEI-LA NP showed a slight decrease in siRNA COM distance and a significant alignment of the two siRNAs, forming almost parallel orientation as the NP detached from the membrane. The results indicate that PEI-LA NP was able to better retain its integrity compared with native PEI NP, consistent with observations from EMSA experiments.

Sun et al.[25] previously explored the complexation mechanism for NPs derived from lipid-substituted PEIs using MD simulations, and found a high degree of correlation between the length of lipid chain and stability of the NPs; long-chained LA led to a more compact structure as compared to short-chain caprylic acid. Fig. S4 shows lipid associations between PEIs of PEI-LA NPs during penetration into the

membranes. Lipid associations was quantified based on the number of pairs of lipid Cs that are closer than 5 Å between each pair of PEIs. Here, lipid association was formed only between the bridging PEI-2 and peripheral PEI-5. The associations follow a decreasing trend, where during detachment, associations were completely lost in the POPC membrane, while it was strongly weakened in the POPS membrane. Since in practical application excessive polymer will be used to form the NP with siRNA, associations are expected to occur between more pairs of PEI-LAs. To disintegrate the PEI-LA NP, these extra lipid associations need to be weakened and broken first, which requires stronger force and larger energy. These lipid associations therefore provide an additional protection mechanism against dissociation of PEI-LA NP, while PEI NP lacks this extra protection.

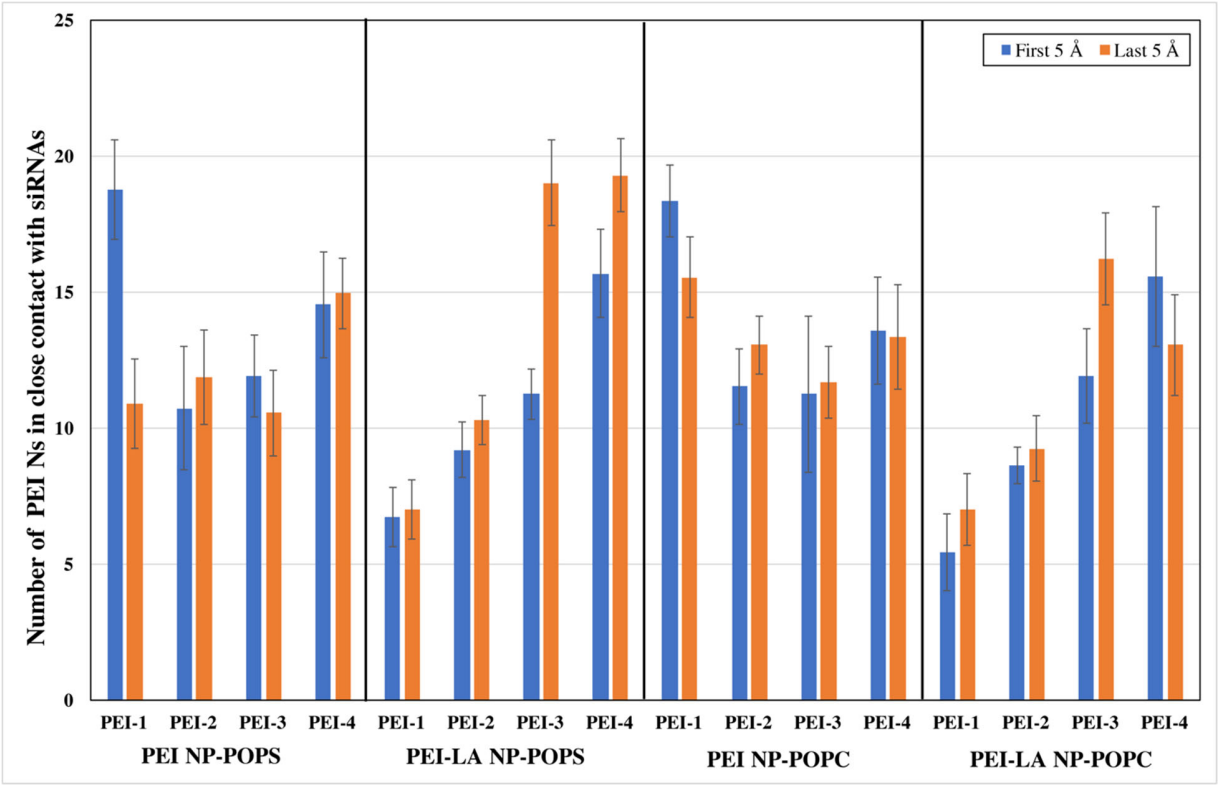

Figure 10. Average number of Ns of bridging PEIs within 4 Å of siRNAs N/O atoms during the first and last 5 Å of the penetration

The anionic lipid molecules abundant in cell membranes may also contribute to dissociation of NPs within the cytoplasm, given that when NPs undergo endocytosis, a layer of encapsulating lipid bilayer will be formed around them [69]. Some NPs may also employ direct penetration to enter the cells through various methods involving diffusion, permeation and pore formation [33]. Upon NP entry into cells, siRNAs need to be released from their carriers for the Argonauts proteins and guide strand of siRNA to form RNA-induced silencing complex (RISC)[70]. Presence of POPS lipids might contribute to disintegration of NPs during endosomal escape. It has been reported that the percentage of PS lipids varies from being ~8.5% in the early endosome to 2.5-3.9 % in the late endosome[71]. Unlike dissociation during cell entry, NP dissociation during endosomal escape can be beneficial to release the NAs for transport to appropriate sub-cellular sites. Our SMD simulations showed that anionic POPS membrane substantially disturb the integrity of siRNA/PEI NPs especially at the end of its membrane crossing and this methodology may help to understand lipids that contribute to release of siRNA in cytoplasm.

Cell membranes have different lipid contents whose lipids exhibit different levels of saturation, chain length and hydrophobicity that determine final biophysical properties of the membrane. For example, the thickness and ordering of the hydrophobic region of the membrane depends on the length and degree of saturation of the lipid tails[72]. Unsaturated lipids occupy a larger volume than saturated lipids due to double bonds inducing a "twist" in the middle of the chain[73]. Saturated lipids display more compact configuration compared with unsaturated lipids, causing saturated lipids to have a higher phase transition temperature. Further studies are necessary to evaluate NP integrity during its penetration into these membranes to obtain a comprehensive picture of the effect of membranes' lipid tails in the membrane.

A more realistic representative of the cell membrane would be a mixture of various lipid species. The major lipid component of eukaryotic membranes are glycerophospholipids including PC, PE, PS, phosphatidylinositiol (PI), and phosphatidic acid (PA) [71]. However, depending on the cell type as well as region of the cell membrane, certain lipid type may be more dominant than others. As a representative example, Koichi et al. [74] investigated the lipid components of two different regions of an intestinal epithelial cell membrane. They found that major lipid content of microvillus membranes was 49% PE and 25.1% PC,

while the percentage for the basolateral membrane was 51% PC and 27.4 % PE. Presence of different lipid head groups affect the curvature of cell membrane. The inclusion of PE in PC bilayer inflicts a curvature onto the membrane, which is used for budding, fission and fusion[75]. Another factor that imposes curvature in membranes is the asymmetric distribution of various lipids between the bilayer leaflets [75]. Presence of other lipids is bound to affect the interaction of NP with lipidic membranes. Simulations studies have been performed to investigate interaction of polymers with a mixture of lipidic membranes [76,77]. However, the mixtures were limited to two lipids and their relative ratio were chosen rather arbitrarily. Additionally, no simulation study was performed on the interaction of the mixture of lipids with NP carriers and NA. Simulations of such complex systems will be beneficial, yet challenging especially due to the lack of exact information on the composition and configuration of the lipid molecules in target cells.

Another factor that might affect integrity of PEI/siRNA NPs is liposomes' size. However, with increase in liposomes' size, other effects including wrapping of NP, aggregation, pore formation, and deformation of liposomes might occur that needs to be systematically evaluated. Here, we have used liposomes with relatively similar size as NPs to prevent aforementioned effects. It is of interest to evaluate the effect of liposomes' size on the stability of both PEI/siRNA NPs and liposomes, which will be addressed in future studies.

Although MD and SMD simulations provide molecular level insight, which is inaccessible through common experimental tools, current computing resources do not permit the length and time scales required to study the dynamics of complex biological systems. The size of our simulated NPs was ~3 nm, while the size of polymeric NPs for NA delivery is reported in the 100- 200 nm range[57]. Direct quantitative comparisons between the experimental observations and simulation results may not be practical. However, qualitatively, our simulations correlate well with experiments, both in terms of the stronger dissociation potential of POPS membranes, and the enhanced stability of PEI-LA NPs.

5 Conclusions

Using a combination of experiments and SMD simulations, integrity and configurational changes of siRNA/PEI NPs were assessed during their interaction with model membranes derived from POPC and POPS. We investigated two polymeric carriers for siRNA delivery, unmodified and LA-substituted PEIs. Binding experiments showed that at the same PEI/siRNA weight ratio, siRNA bound better with the PEI compared with PEI-LA, and higher polymer:NA ratio was required for LA-modified PEIs to provide full siRNA binding. POPS liposomes induced partial dissociation of both types of NPs whereas POPC liposomes lacked such an ability. SMD simulations showed that the NPs had stronger interactions with the POPS than with POPC membrane, evidenced by the formation of more HBs with the POPS membrane. Consequently, larger structural changes were experienced by the PEI NP penetrating the POPS membrane, showing signs of NP destabilization. In addition, we found that lipid substitution on PEIs enhanced the stability of the NPs during membrane discharge. Lipid association among PEIs of PEI-LA NP as well as parallel orientation between its siRNAs provide an additional protection against the NP disintegration. Our complementary experimental and simulations data provide a unique insight into integrity and configurational changes of siRNA/PEI NPs during membrane crossing, which can facilitate the design of more efficient carrier for NA delivery.

Conflict of Interest

Dr. Uludag is the scientific founder and shareholder in a spin-off company (RJH Biosicences Inc.) intended to develop the lipopolymers for biomedical applications.

Acknowledgments

Compute Canada and Westgrid are gratefully acknowledged for providing the computing resources and technical support. This work is funded by Natural Sciences and Engineering Research Council of Canada (NSERC), Canadian Institutes of Health Research (CIHR) and Alberta Innovates-Technology Futures (AITF). We thank Dr. A. Lavasanifar (Faculty of Pharmacy & Pharmaceutical Sciences, Univ. of Alberta) for access to the Zetasizer.

References

1 D. Pezzoli, E. K. Tsekoura, K. C. R. Bahadur, G. Candiani, D. Mantovani and H. Uludağ, *Sci. China Mater.*, 2017, **60**, 529–542.

2 S. K. Samal, M. Dash, S. Van Vlierberghe, D. L. Kaplan, E. Chiellini, C. Van Blitterswijk, L. Moroni and P. Dubruel, *Chem. Soc. Rev.*, 2012, **41**, 7147–7194.

3 J. Sabín, C. Vázquez-Vázquez, G. Prieto, F. Bordi and F. Sarmiento, *Langmuir*, 2012, **28**, 10534–10542.

4 K. Utsuno, H. Kono, E. Tanaka, N. Jouna, Y. Kojima and H. Uludağ, *Chem. Pharm. Bull.*, 2016, **64**, 1484–1491.

5 D. Meneksedag-Erol, T. Tang and H. Uludağ, *Biomaterials*, 2018, **156**, 107–120.

6 M. Laurencin, T. Georgelin, B. Malezieux, J.-M. Siaugue and C. Ménager, *Langmuir*, 2010, **26**, 16025–16030.

7 M. Boeckle, S. , von Gersdorff, K. , van der Piepen, S. , Culmsee, C. , Wagner, E. and Ogris, *J. Gene Med.*, 2004, **6**, 1102–1111.

8 C. Zhang, F.-G. Wu, P. Hu and Z. Chen, *J. Phys. Chem. C*, 2014, **118**, 12195–12205.

9 K. Yasuhara, M. Tsukamoto, Y. Tsuji and J. Kikuchi, *Colloids Surfaces A Physicochem. Eng. Asp.*, 2012, **415**, 461–467.

10 R. Jahn, T. Lang and T. C. Südhof, *Cell*, 2003, **112**, 519–533.

11 S. R. Clark, K. Y. Lee, H. Lee, J. Khetan, H. C. Kim, Y. H. Choi, K. Shin and Y.-Y. Won, *Acta Biomater.*, 2018, **65**, 317–326.

12 S. Hong, P. R. Leroueil, E. K. Janus, J. L. Peters, M.-M. Kober, M. T. Islam, B. G. Orr, J. R. Baker and M. M. Banaszak Holl, *Bioconjug. Chem.*, 2006, **17**, 728–734.

13 U. Kwolek, D. Jamr??z, M. Janiczek, M. Nowakowska, P. Wydro and M. Kepczynski, *Langmuir*, 2016, **32**, 5004–5018.

14 C. K. Choudhury, A. Kumar and S. Roy, *Biomacromolecules*, 2013, **14**, 3759–3768.

15 L. Kjellen and U. Lindahl, *Annu. Rev. Biochem.*, 1991, **60**, 443–475.

16 T. Miller, M. C. Goude, T. C. McDevitt and J. S. Temenoff, *Acta Biomater.*, 2014, **10**, 1705–1719.

17 I. Moret, J. E. Peris, V. M. Guillem, M. Benet, F. Revert, F. Dasí, A. Crespo and S. F. Aliño, *J. Control. Release*, 2001, **76**, 169–181.

18 A. Kwok and S. L. Hart, *Nanomedicine Nanotechnology, Biol. Med.*, 2011, **7**, 210–219.

19 N. Ernst, S. Ulrichskötter, W. A. Schmalix, J. Rädler, R. Galneder, E. Mayer, S. Gersting, C. Plank, D. Reinhardt and J. Rosenecker, *J. Gene Med. A cross-disciplinary J. Res. Sci. gene Transf. its Clin. Appl.*, 1999, **1**, 331–340.

20 A. A. Gurtovenko, *J. Phys. Chem. B*.

21 P. Chen, Z. Huang, J. Liang, T. Cui, X. Zhang, B. Miao and L.-T. Yan, *ACS Nano*, 2016, **10**, 11541–11547.

22 G. Zhu, Z. Huang, Z. Xu and L.-T. Yan, *Acc. Chem. Res.*, 2018, **51**, 900–909.

23 P. Chen, H. Yue, X. Zhai, Z. Huang, G.-H. Ma, W. Wei and L.-T. Yan, *Sci. Adv.*, 2019, **5**, eaaw3192.

24 H. M. Aliabadi, B. Landry, R. K. Bahadur, A. Neamnark, O. Suwantong and H. Uludağ, *Macromol. Biosci.*, 2011, **11**, 662–672.

25 C. Sun, T. Tang and H. Uludag, *Biomaterials*, 2013, **34**, 2822–2833.

26 A. Neamnark, O. Suwantong, R. B. K. C., C. Y. M. Hsu, P. Supaphol and H. Uludağ, *Mol. Pharm.*, 2009, **6**, 1798–1815.

27 M. Abbasi, H. M. Aliabadi, E. H. Moase, A. Lavasanifar, K. Kaur, R. Lai, C. Doillon and H. Uludağ, *Pharm. Res.*, 2011, **28**, 2516–2529.

28 K. Utsuno and H. Uludağ, *Biophys. J.*, 2010, **99**, 201–207.

29 A. von Harpe, H. Petersen, Y. Li and T. Kissel, *J. Control. Release*, 2000, **69**, 309–322.

30 J. Suh, H. Paik and B. K. HwANG, *Bioorg. Chem.*, 1994, **22**, 318–327.

31 J. Nagaya, M. Homma, A. Tanioka and A. Minakata, *Biophys. Chem.*, 1996, **60**, 45–51.

32 G. J. M. Koper, R. C. van Duijvenbode, D. D. P. W. Stam, U. Steuerle and M. Borkovec, *Macromolecules*, 2003, **36**, 2500–2507.

33 Y. Nademi, T. Tang and H. Uludağ, *Nanoscale*, 2018, **10**, 17671–17682.

34 E. L. Wu, X. Cheng, S. Jo, H. Rui, K. C. Song, E. M. Dávila-Contreras, Y. Qi, J. Lee, V. Monje-Galvan and R. M. Venable, *J. Comput. Chem.*, 2014, **35**, 1997–2004.

35 B. R. Brooks, C. L. Brooks III, A. D. Mackerell Jr, L. Nilsson, R. J. Petrella, B. Roux, Y. Won, G. Archontis, C. Bartels and S. Boresch, *J. Comput. Chem.*, 2009, **30**, 1545–1614.

36 S. Jo, T. Kim, V. G. Iyer and W. Im, *J. Comput. Chem.*, 2008, **29**, 1859–1865.

37 W. L. Jorgensen, *J. Am. Chem. Soc.*, 1981, **103**, 335–340.

38 J. Lee, X. Cheng, J. M. Swails, M. S. Yeom, P. K. Eastman, J. A. Lemkul, S. Wei, J. Buckner, J. C. Jeong and Y. Qi, *J. Chem. Theory Comput.*, 2015, **12**, 405–413.

39 S. Park, F. Khalili-Araghi, E. Tajkhorshid and K. Schulten, *J. Chem. Phys.*, 2003, **119**, 3559–3566.

40 Q. Wei, W. Zhao, Y. Yang, B. Cui, Z. Xu and X. Yang, *ChemPhysChem*, 2018, **210009**, 1–14.

41 H. Nguyen, N. Do, T. Phan and T. Pham, *Appl. Biochem. Biotechnol.*, 2018, **184**, 401–413.

42 Y. Xu, J. Shen, X. Luo, I. Silman, J. L. Sussman, K. Chen and H. Jiang, *J. Am. Chem. Soc.*, 2003, **125**, 11340–11349.

43 D. J. Brockwell, E. Paci, R. C. Zinober, G. S. Beddard, P. D. Olmsted, D. A. Smith, R. N. Perham and S. E. Radford, *Nat. Struct. Mol. Biol.*, 2003, **10**, 731.

44 S. Azadi, M. Tafazzoli-Shadpour and R. Omidvar, *Mol. Biol.*, 2018, **52**, 723–731.

45 H. Lu and K. Schulten, *Proteins Struct. Funct. Bioinforma.*, 1999, **35**, 453–463.

46 E. J. Denning, U. D. Priyakumar, L. Nilsson and A. D. Mackerell, *J. Comput. Chem.*, 2011, **32**, 1929–1943.

47 J. B. Klauda, R. M. Venable, J. A. Freites, J. W. O'Connor, D. J. Tobias, C. Mondragon-Ramirez, I. Vorobyov, A. D. MacKerell and R. W. Pastor, *J. Phys. Chem. B*, 2010, **114**, 7830–7843.

48 J. C. Phillips, R. Braun, W. Wang, J. Gumbart, E. Tajkhorshid, E. Villa, C. Chipot, R. D. Skeel, L. Kalé and K. Schulten, *J. Comput. Chem.*, 2005, **26**, 1781–1802.

49 T. Darden, D. York and L. Pedersen, *J. Chem. Phys.*, 1993, **98**, 10089–10092.

50 J.-P. Ryckaert, G. Ciccotti and H. J. . Berendsen, *J. Comput. Phys.*, 1977, **23**, 327–341.

51 G. J. Martyna, D. J. Tobias and M. L. Klein, *J. Chem. Phys.*, 1994, **101**, 4177–4189.

52 S. E. Feller, Y. Zhang, R. W. Pastor and B. R. Brooks, *J. Chem. Phys.*, 1995, **103**, 4613–4621.

53 W. Humphrey, A. Dalke and K. Schulten, *J. Mol. Graph.*, 1996, **14**, 33–38.

54 D. Meneksedag-Erol, T. Tang and H. Uludağ, *J. Phys. Chem. B*, 2015, **119**, 5475–5486.

55 J. Ziebarth and Y. Wang, *Biophys. J.*, 2009, **97**, 1971–1983.

56 C. Sun, T. Tang, H. Uludağ and J. E. Cuervo, *Biophys. J.*, 2011, **100**, 2754–2763.

57 H. M. Aliabadi, B. Landry, C. Sun, T. Tang and H. Uludağ, *Biomaterials*, 2012, **33**, 2546–

2569.

58 M. Sud, E. Fahy, D. Cotter, A. Brown, E. A. Dennis, C. K. Glass, A. H. Merrill, R. C. Murphy, C. R. H. Raetz, D. W. Russell and S. Subramaniam, *Nucleic Acids Res.*, 2007, **35**, D527–D532.

59 G. Caracciolo and H. Amenitsch, *Eur. Biophys. J.*, 2012, **41**, 815–829.

60 R. Dias, M. Rosa, A. C. Pais, M. Miguel and B. Lindman, *J. Chinese Chem. Soc.*, 2004, **51**, 447–469.

61 G. Caracciolo, D. Pozzi, H. Amenitsch and R. Caminiti, *Langmuir*, 2007, **23**, 8713–8717.

62 Y. Xu and F. C. Szoka, *Biochemistry*, 1996, **35**, 5616–5623.

63 G. Caracciolo, D. Pozzi, R. Caminiti, C. Marchini, M. Montani, A. Amici and H. Amenitsch, *Appl. Phys. Lett.*, 2007, **91**, 143903.

64 G. Caracciolo, C. Marchini, D. Pozzi, R. Caminiti, H. Amenitsch, M. Montani and A. Amici, *Langmuir*, 2007, **23**, 4498–4508.

65 M. Langner and K. Kubica, *Chem. Phys. Lipids*, 1999, **101**, 3–35.

66 D. Bach, E. Wachtel, N. Borochov, G. Senisterra and R. M. Epand, *Chem. Phys. Lipids*, 1992, **63**, 105–113.

67 K. L. Koster, M. S. Webb, G. Bryant and D. V Lynch, *Biochim. Biophys. Acta (BBA)-Biomembranes*, 1994, **1193**, 143–150.

68 D. Meneksedag-Erol, T. Tang and H. Uludağ, *Biomaterials*, 2014, **35**, 7068–7076.

69 S. Zhang, H. Gao and G. Bao, *ACS Nano*, 2015, **9**, 8655–8671.

70 B. Czech and G. J. Hannon, *Nat. Rev. Genet.*, 2011, **12**, 19.

71 P. A. Leventis and S. Grinstein, , DOI:10.1146/annurev.biophys.093008.131234.

72 P. A. Janmey and P. K. J. Kinnunen, *Trends Cell Biol.*, 2006, **16**, 538–546.

73 B. Antonny, , DOI:10.1016/j.devcel.2012.10.009.

74 K. Koichi, F. Michiya and N. Makoto, *Biochim. Biophys. Acta (BBA)-Lipids Lipid Metab.*, 1974, **369**, 222–233.

75 G. Van Meer, D. R. Voelker and G. W. Feigenson, *Nat. Rev. Mol. cell Biol.*, 2008, **9**, 112.

76 A. Y. Kostritskii, D. A. Kondinskaia, A. M. Nesterenko and A. A. Gurtovenko, *Langmuir*, 2016, **32**, 10402–10414.

77 C. D. Lorenz, J. Faraudo and A. Travesset, *Langmuir*, 2008, **24**, 1654–1658.